NASA TECHNICAL
MEMORANDUM

NASA TM X-64539

# DESIGN AND DEVELOPMENT OF A LUNAR RADIOMETER

By Walter Fountain
Space Sciences Laboratory

July 28, 1970



NASA

*George C. Marshall Space Flight Center*
*Marshall Space Flight Center, Alabama*

TECHNICAL REPORT STANDARD TITLE PAGE

| 1. REPORT NO. | 2. GOVERNMENT ACCESSION NO. | 3. RECIPIENT'S CATALOG NO. |
|---|---|---|
| TM X-64539 | | |

| 4. TITLE AND SUBTITLE | 5. REPORT DATE |
|---|---|
| Design and Development of a Lunar Radiometer | July 28, 1970 |
| | 6. PERFORMING ORGANIZATION CODE |
| 7. AUTHOR(S) | 8. PERFORMING ORGANIZATION REPORT # |
| Walter Fountain | |
| 9. PERFORMING ORGANIZATION NAME AND ADDRESS | 10. WORK UNIT NO. |
| George Marshall Space Flight Center<br>Marshall Space Flight Center, Alabama 35812 | 11. CONTRACT OR GRANT NO. |
| | 13. TYPE OF REPORT & PERIOD COVERED |
| 12. SPONSORING AGENCY NAME AND ADDRESS | Technical Memorandum |
| | 14. SPONSORING AGENCY CODE |

15. SUPPLEMENTARY NOTES

Prepared by Space Sciences Laboratory,
Science and Engineering Directorate.

16. ABSTRACT

This report describes the design and presents a performance analysis of an infrared radiometer built by the Space Sciences Laboratory. The infrared radiometer is used with an astronomical telescope in the study of thermal emission from the moon. Calibration and data reduction equations are given, and an error analysis performed for data obtained with the system is presented.

| 17. KEY WORDS | 18. DISTRIBUTION STATEMENT |
|---|---|
| Infrared radiometer<br>Astronomical telescope<br>Thermal emission<br>Calibration and data reduction<br>Error analysis<br>Lunar temperatures | ANNOUNCE IN STAR.<br>Walter Fountain |

| 19. SECURITY CLASSIF. (of this report) | 20. SECURITY CLASSIF. (of this page) | 21. NO. OF PAGES | 22. PRICE |
|---|---|---|---|
| Unclassified | Unclassified | 44 | $3.00 |

MSFC - Form 3292 (May 1969)

# TABLE OF CONTENTS

# LIST OF ILLUSTRATIONS



# LIST OF TABLES

# LIST OF SYMBOLS

| Symbol | Definition |
|---|---|
| $A_c$ | area of calibration source aperture |
| $A_d$ | area of detector |
| $A_t$ | area of telescope objective |
| $D_t$ | diameter of telescope objective |
| $D_\lambda^*$ | spectral detectivity of detector at wavelength $\lambda$ |
| d | distance between calibration blackbody and detector |
| E' | image intensity of optical system |
| $F_n$ | focal ratio of optical system, $F_n = \frac{f}{D}$ |
| $f_t$ | focal length of telescope |
| $N_\lambda(\lambda, T)$ | spectral radiance of blackbody at temperature T |
| N(T) | effective target radiance — integral of the target spectral radiance weighted by the system relative spectral response; target is assumed to be a black or gray body |
| $N(T_m)$ | effective radiance of moon at temperature $T_m$ |
| $\overline{N}_T(\text{eff})$ | effective target radiance — integral of the target spectral radiance weighted by the detector relative spectral response |
| $\overline{N}_T'(\text{eff})$ | system noise equivalent radiance — that value of effective target radiance which gives rise to a signal-to-noise ratio of 1 |
| $NEP_\lambda$ | noise equivalent power of detector at wavelength $\lambda$ |
| $P_d$ | absolute power incident on detector |

# LIST OF SYMBOLS (Continued)

| Symbol | Definition |
|---|---|
| $P_d(\text{eff})$ | power incident on detector weighted by detector's relative spectral response |
| Rc | calibration constant |
| $R_\lambda(\lambda)$ | spectral responsivity of a given detector |
| $RR_\lambda$ | relative spectral response of a detector |
| $\frac{R_\lambda}{R_{\lambda_p}}$ | spectral response of system normalized to unity at a wavelength of peak response |
| S | signal output |
| S/N | rms signal-to-noise ratio |
| T | absolute temperature in degrees Kelvin |
| $T_{min}$ | system minimum detectable temperature |
| $V_{BG}$ | voltage contribution because of background radiation while viewing calibration source 1 |
| $V_{c_1}$ | voltage contribution because of calibration source 1 |
| $V_{c_2}$ | voltage contribution because of calibration source 2 |
| $V_I$ | voltage because of radiation received from an internal reference source |
| $V_T$ | $(V_{c_1} + V_{BG})$, sum of voltage contributions from calibration source 1 and associated background radiation |
| $V_S$ | voltage because of sky radiation |

# LIST OF SYMBOLS (Concluded)

| Symbol | Definition |
|---|---|
| $V_m$ | voltage output because of the moon alone, $(V_{m+s} - V_m)$ |
| $V_{m+s}$ | sum of voltage contributions from the moon and sky |
| $\alpha$ | Fourier coefficient of chop waveform fundamental |
| $\Delta T_{min}$ | system minimum detectable temperature difference |
| $\Delta V_c$ | rms voltage difference between calibration blackbodies, $(V_1 - V_2)$ |
| $\Delta f$ | electrical bandwidth |
| $\epsilon(\lambda)$ | spectral emissivity |
| $\overline{\epsilon}$ | average emissivity over a given spectral band |
| $\rho_o$ | reflectivity of optical element |
| $\rho_c$ | reflectivity of chopper mirror |
| $\rho_t^2$ | product of reflectivity of primary and secondary mirrors of Cassegrainian optical system |
| $\tau_a(\lambda)$ | spectral atmospheric transmission |
| $\overline{\tau}_a$ | average atmospheric transmission over a given spectral band |
| $\tau_f(\lambda)$ | actual filter transmission |
| $\overline{\tau}_f$ | average filter transmission over a given spectral band |
| $\tau_w(\lambda)$ | actual transmission of dewar window (usually KRS-5) |

TECHNICAL MEMORANDUM X-64539

# DESIGN AND DEVELOPMENT OF A LUNAR RADIOMETER

## SUMMARY

A focal plane radiometer for measuring lunar brightness temperature was designed and constructed. The system utilizes a Ge:Hg detector, filtered spectrally around a narrow band of wavelengths and centered at 11 micrometers ($\mu$m). The system was designed to use an f/16 astronomical telescope as its collecting optics and is expected to detect temperatures on the lunar surface as low as 118°K. An error analysis shows that absolute temperatures around the subsolar temperature may be measured to within an accuracy of ±7.9°K with the calibration and data reduction techniques described.

Several scans of the lunar disc near the full moon phase using the 30-cm reflector of the Space Sciences Laboratory are shown. Additional lunar measurements and a description of atmospheric transmission measurements will be presented in a later report.

## INTRODUCTION

An infrared (IR) radiometer has been designed to make brightness temperature measurements of extended sources in the solar system, and it may be useful in studying certain infrared stellar objects such as R-Monocerotis or the Magellenic clouds also. The instrument was designed to utilize an f/16 Cassegrain telescope as its collecting optics.

The main object of study in the solar system will be the moon. Using the 30-cm telescope of the Space Sciences Laboratory, the system angular resolution of approximately 21 arc sec will allow measurements from selected areas of about 40 km diameter. Using the Marshall Space Flight Center 1.5-meter telescope at Tucson will give an angular resolution of 4.5 arc sec, which corresponds to a spot of about 9 km on the moon. Measurements of infrared radiation from the planets are possible, but are of a limited nature because of the relatively large field of view of the system.

The system makes infrared measurements in a 2-$\mu$m bandpass centered near 11 $\mu$m. Since the peak emission of a 264°K blackbody occurs at approximately 11 $\mu$m, this might imply that the temperatures of the objects of interest are expected to be in this range only. However, any object with sufficient emission in this region may be a candidate for study; for example, the sun. The selection of the 11-$\mu$m region as a design specification was determined by the desire to minimize the effects of reflected solar radiation, to take advantage of the excellent atmospheric window in this spectral region, and to facilitate the conversion of radiance measurements to brightness temperatures.

# RADIOMETER DESIGN

## Detector Selection and Optical Design

The first concern in the design of a radiometer is a determination of the approximate strength and wavelength band of the signal to be measured. These are necessary criteria for the selection of detector, filters, windows, and other optical components. A cursory review of the literature [1] reveals that the dynamic range of radiation from an area of the lunar surface may be approximated by an extended blackbody source at temperatures of 400°K for full moon and about 100°K for new moon. This places the spectral emission peaks at wavelengths of 7.2 $\mu$m and 28.9 $\mu$m, respectively. This indicates that if a single detector is to be used for both lunar daytime and nighttime measurements, it would require adequate spectral responsivity covering a large wavelength interval.

Of the two basic types of detectors available, thermal and photodetective, the photodetective type is considered most appropriate to meet all the goals of a spatial scanning type of measurement, where system response time is an important parameter. The shorter time constant of the photodetective element allows greater latitude in experiment design and data acquisition techniques.

Three commercially available photodetective detectors were considered, all theoretically capable of background noise limited performance. These were the copper-doped germanium (Ge:Cu), mercury-doped germanium (Ge:Hg), and mercury-cadmium-telluride (Hg:Cd:Te) detectors. Typical spectral response curves for these detectors are shown in Figure 1. The Ge:Cu and Ge:Hg detectors become sensitive to IR radiation when cooled to

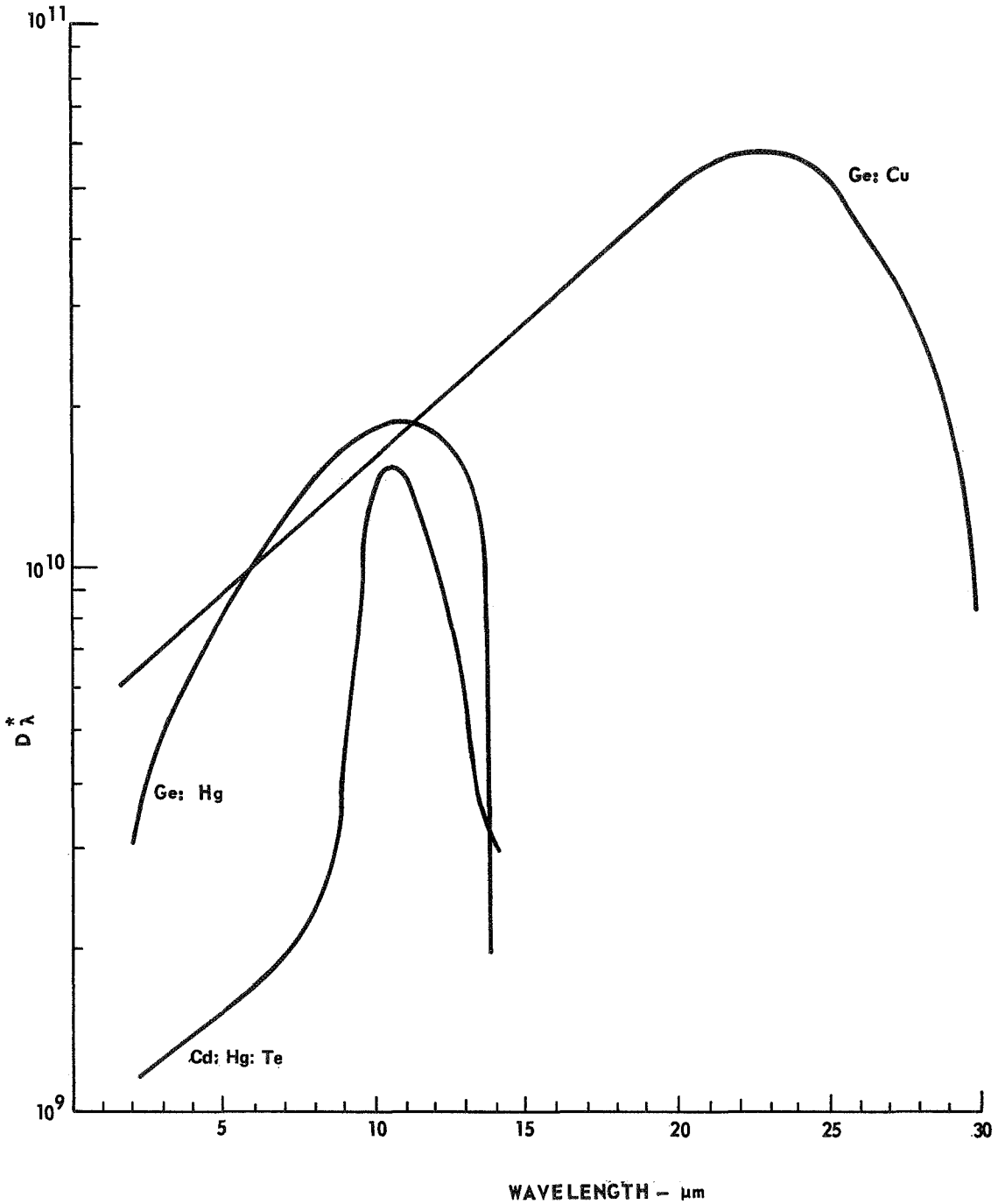


Figure 1. Spectral D* for Ge:Hg, Ge:Cu, and Hg:Cd:Te detectors.

temperatures below 20°K, while the Hg:Cd:Te becomes sensitive at 77°K. Since these detectors require cryogenic cooling, design requirements must include considerations of specific dewar configuration, dimensions, and coolant hold times.

Consideration of the atmospheric effects upon radiation that is incident upon the earth from extraterrestrial sources is necessary for guidance in bandpass filter selection as well as in signal strength calculations. A number of investigators have studied and measured the properties of the atmosphere as a function of wavelength for various values of pressure, humidity, altitude, and haze conditions. A characteristic absorption curve for a vertical path through the atmosphere at sea level is shown in Figure 2. This plot shows two general transmission bands that fall within the waveband of interest; an excellent band between about 10 and 12 $\mu$m and another weaker band between 16 and 24 $\mu$m. The 16- to 24-$\mu$m band is structured with strong water vapor absorption bands that lose their strength only at extremely high altitudes. A strong $O_3$ absorption band occurs at approximately 9.6 $\mu$m.

Using the 400°K and 100°K values and taking into account the atmospheric effects, one can approximate with sufficient accuracy the radiant power extremes available, within a given spectral interval, to a detector placed in the focal plane of a given telescope. The results of this exercise combined with consideration of detector capabilities led to the decision to select the Ge:Hg detector and to limit measurements to the 10- to 12-$\mu$m band. A schematic of the detector/dewar system is shown in Figure 3.

The insert in Figure 3 shows the removable detector/aperture unit, designed to provide a cold shield for an unvignetted detector field of approximately 4 deg. The detector field is thus closely matched to the convergence angle of an f/16 optical system.

The optical path of the radiometer is shown schematically in Figure 4. Radiation from the telescope optics is reflected off the chopper, passes through the KRS-5 window and the interference filter, and is focused at the detector surface A. When the two-bladed chopper is in the open position, the detector views a reference blackbody, the radiation from the telescope is focused at position B where an aperture in a viewing and photographic mirror defines the field of view of a 1P21 photomultiplier tube. This channel is used to aid in visually correlating the lunar features with the infrared signal. Transfer optics reimage the telescope image at point C, where either an eyepiece or a camera may be mounted.

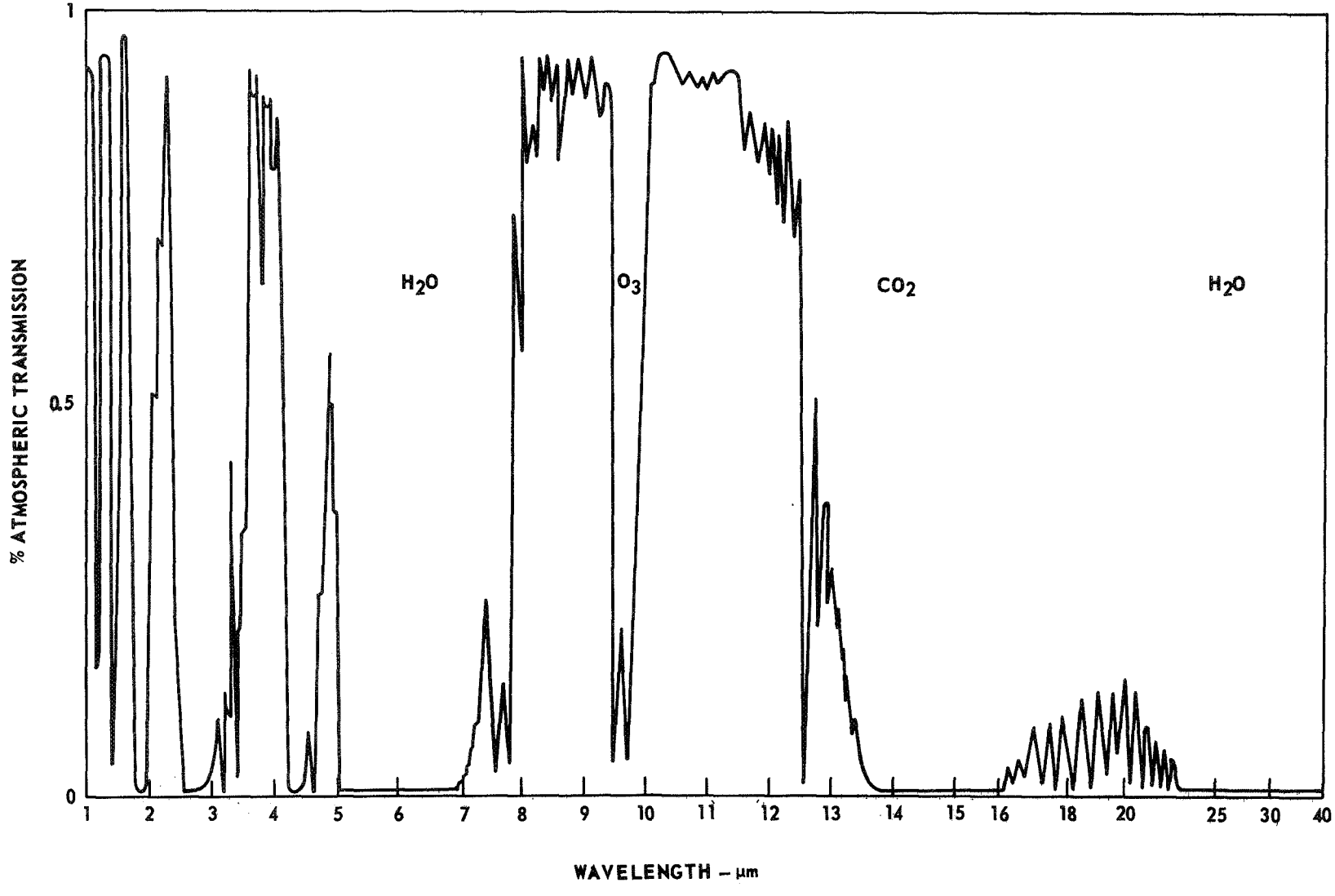


Figure 2. Atmospheric transmission, 1 through 40 $\mu$m.

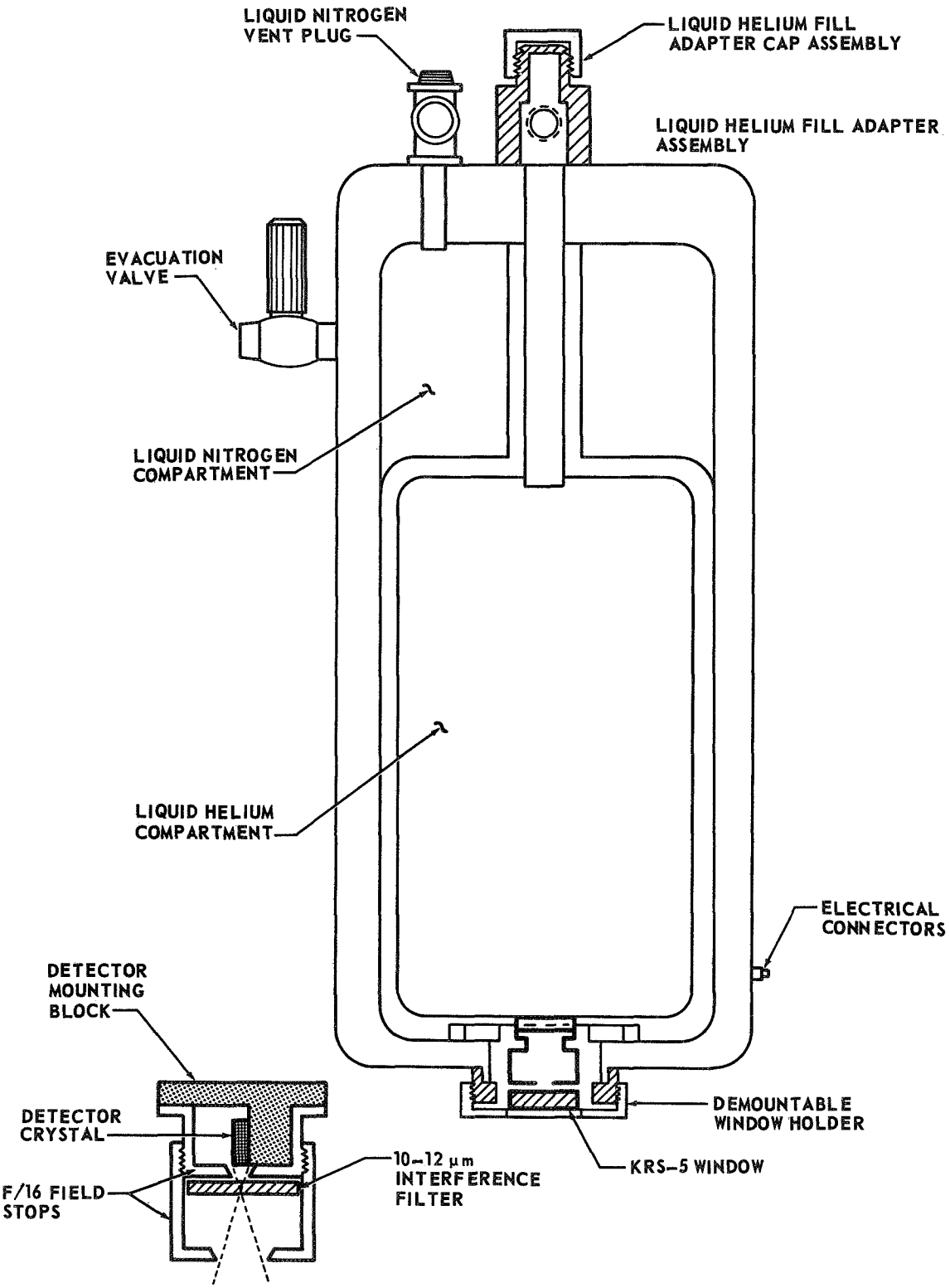


Figure 3. Schematic of detector/dewar.

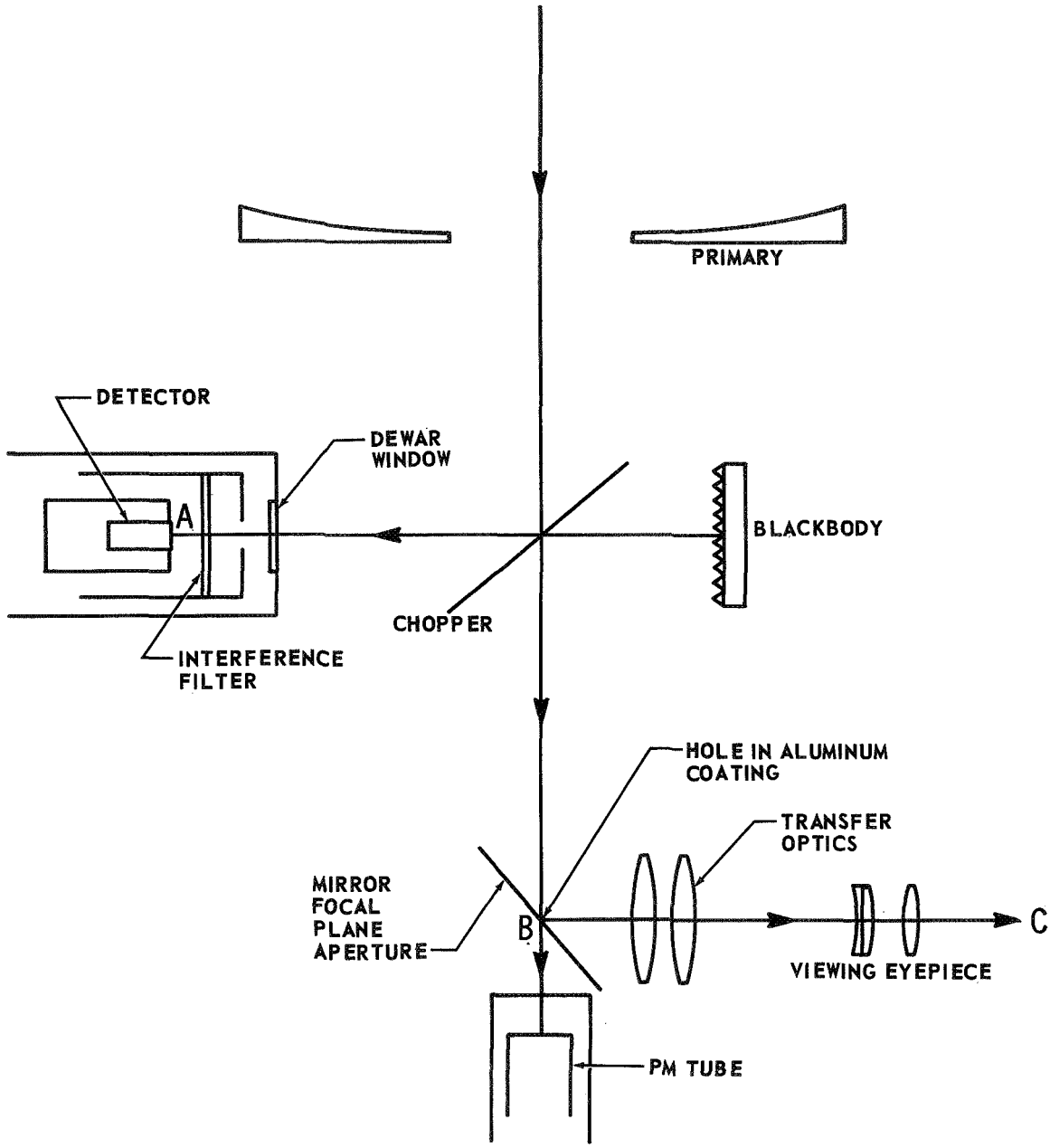


Figure 4. Optical path of radiometer.

## General Performance Analysis

Having selected the Ge:Hg detector for the 10- to 12-$\mu$m lunar measurements, the characteristics of this detector may be used to evaluate certain system characteristics, such as minimum detectable temperature and minimum detectable temperature difference.

The telescope image irradiance E' from a distant extended graybody source, viewed through the atmosphere, is given by

$$E' = \frac{A_t}{f_t^2} \int_{\lambda_1}^{\lambda_2} N_\lambda(\lambda, T) \cdot \tau_a(\lambda) \cdot \rho_o^2(\lambda) \cdot \epsilon(\lambda)\, d\lambda , \qquad (1)$$

where $\lambda_1$ and $\lambda_2$ are the wavelength limits of interest, and $N_\lambda(\lambda, T)$ is the spectral radiance of the source at temperature T.

The absolute power to a detector placed in the focal plane of a telescope is weighted by the spectral transmission of filters, windows, and reflectance of any transfer or chopper mirrors in the optical path. These factors are included in the following equation for the power on a detector of area $A_d$:

$$P_d = \frac{A_t}{f_t^2} \cdot A_d \int_0^\infty N_\lambda(\lambda, T) \cdot \tau_a(\lambda) \cdot \rho_o^2(\lambda) \cdot \epsilon(\lambda) \cdot \tau_f(\lambda) \cdot \tau_w(\lambda) \cdot \rho_c(\lambda)\, d\lambda . \qquad (2)$$

The output signal voltage is determined by the spectral distribution of the radiant power incident on the detector weighted by the spectral responsivity, $R_\lambda(\lambda)$, of the particular detector used. Thus,

$$S = \frac{A_t}{f_t^2} \cdot A_d \int_0^\infty R_\lambda(\lambda) \cdot N_\lambda(\lambda, T) \cdot \tau_a(\lambda) \cdot \rho_o^2(\lambda) \cdot \rho_c(\lambda) \cdot \tau_f(\lambda) \cdot \tau_w(\lambda)\, \epsilon(\lambda)\, d\lambda . \qquad (3)$$

In many cases, for a preliminary system analysis, it is necessary to use published manufacturer's data for detector performance for filter and window transmissions, etc. and to use best estimates for such factors as $\tau_a$ and optical system parameters. The analysis is simplified by rewriting equation (3) as

$$S \sim P_d(\text{eff}) = \frac{A_t}{f_t^2} \cdot A_d \cdot \overline{\tau}_f \cdot \overline{\tau}_w \cdot \overline{\tau}_a \cdot \overline{\rho}_o^2 \cdot \overline{\epsilon} \int_{\lambda_1}^{\lambda_2} RR_\lambda \cdot N_\lambda(\lambda, T)\, d\lambda , \qquad (4)$$

where the loss factors are averaged over the spectral bandpass of the system as defined by the cuton and cutoff wavelengths of the interference filter, and $RR_\lambda$ is a characteristic relative spectral response curve of the type of detector to be used.

The expected signal-to-noise ratio for different lunar temperatures may be evaluated from equation (4) if the detector spectral noise equivalent power is known, since for a narrow band system,

$$\frac{S}{N} = \frac{V_S}{V_N} = \frac{P_d(\text{eff})}{NEP_\lambda} \cdot \alpha \qquad (5)$$

Here, $\lambda$ is taken to be the effective wavelength of the narrow band filter used with the system, and $\alpha$ is a factor determined by the waveform of the chopped signal.

Equation (5) may be expressed in terms of such parameters as detector $D^*_\lambda$, electrical bandwidth, and optical system F-number by combining equations (4) and (5) and making the following substitutions:

$$A_t = \frac{\pi D_t^2}{4} \quad , \quad f_t^2 = F_n^2 \cdot D_t^2 \quad ,$$

and

$$NEP_\lambda = \frac{A_d^{1/2} \cdot (\Delta f)^{1/2}}{D^*_\lambda}$$

This leads to a general system performance equation,

$$S/N = \frac{P_d(\text{eff})}{NEP_\lambda} \cdot \alpha = \frac{\pi}{4} \cdot \overline{\tau}_f \cdot \overline{\tau}_w \cdot \overline{\tau}_a \cdot \overline{\rho}_o^{\,2} \cdot \overline{\rho}_c \cdot \overline{\epsilon}_T \cdot D^*_\lambda \cdot \alpha A_d^{1/2} \cdot (\Delta f)^{-1/2} \cdot F_n^{-1/2} \cdot \overline{N}_T(\text{eff}) \quad , \qquad (6a)$$

where

$$\bar{N}_T(\text{eff}) = \int_{\lambda_1}^{\lambda_2} RR_\lambda \cdot N_\lambda(\lambda, T)\, d\lambda \qquad (6b)$$

and is termed the effective target radiance.

The system performance will be evaluated for target temperatures of 200°K and 400°K based on the values listed in Table 1.

TABLE 1. SYSTEM PARAMETERS

| | |
|---|---|
| $\bar{\tau}_f$ | = 0.55 |
| $\bar{\tau}_w$ | = 0.70 |
| $\bar{\tau}_a$ | = 0.90 (10 to 12 $\mu$m) |
| $\bar{\rho}_o^3$ | = $\rho_p \cdot \rho_s \cdot \rho_c = (0.97)^3 = 0.91$ |
| $D^*_\lambda$ | = $2.0 \times 10^{10}$ (field of view = 4 deg, $\Delta f$ = 1 Hz, $\lambda$ = 11 $\mu$m) |
| $A_d^{1/2}$ | = $(1.96 \times 10^{-3}\ \text{cm}^2)^{1/2} = 4.42 \times 10^{-2}$ cm (0.5 mm diameter) |
| $\Delta f$ | = 1 Hz |
| $F_n$ | = 16 |
| $\epsilon$ | = 1 |
| $\alpha$ | = 0.45 |

$\bar{N}_T(\text{eff})$ has been evaluated numerically for T = 200°K and 400°K and found to be

$$\bar{N}_{T_{200}}(\text{eff}) = \int_{\lambda_1=10.2\,\mu\text{m}}^{\lambda_2=12.2\,\mu\text{m}} RR_\lambda \cdot N_\lambda(\lambda, T_{200})\, d\lambda = 2.03 \times 10^{-4}\ \text{watts} \cdot \text{cm}^{-2} \cdot \text{sr}^{-1},$$

and

$$\bar{N}_{T_{400}}(\text{eff}) = \int_{\lambda_1}^{\lambda_2} RR_\lambda \cdot N_\lambda(\lambda, T_{400})\, d\lambda = 5.07 \times 10^{-3} \text{watts} \cdot \text{cm}^{-2} \cdot \text{sr}^{-1} \quad .$$

Equation (6a) may be written as

$$S/N = C \cdot \bar{N}_T(\text{eff}) \quad ,$$

where

$$C = \frac{\pi}{4} \cdot \bar{\tau}_f \cdot \bar{\tau}_w \cdot \bar{\tau}_a \cdot \rho_o^{\,3} \cdot \bar{\epsilon} \cdot D_\lambda^* \cdot A_d^{\,1/2} \cdot \alpha\, f^{1/2} \cdot F_n^{\,-2} = 3.80 \times 10^5 \ \frac{\text{cm}^2 \cdot \text{sr}}{\text{watt}}$$

Thus,

$$S/N\ (200°K) = (3.80 \times 10^5) \times (2.03 \times 10^{-4}) = 7.71 \times 10^1 \quad ,$$

and

$$S/N\ (400°K) = (3.80 \times 10^5) \times (5.07 \times 10^{-3}) = 1.927 \times 10^3 \quad .$$

Thus, it is seen that lunar surface temperatures of 200°K and 400°K should result in signal-to-noise ratios of approximately 77 and 1927, respectively.

The minimum absolute temperature measurable with the system is defined as that temperature which gives rise to an S/N ratio of 1. If equation (6a) is set equal to 1 and solved for $\bar{N}_T(\text{eff})$, the following expression for the system noise equivalent radiance, $\bar{N}_T'(\text{eff})$, is obtained:

$$\bar{N}_T'(\text{eff}) = \frac{1}{C} \qquad (7)$$

Using the same parameters as above, this is computed to be $2.63 \times 10^{-6}$ watts $\cdot$ $cm^{-2} \cdot sr^{-1}$, which corresponds to a radiometric temperature of approximately 118°K. This then would be the $T_{min}$ of the system based on the assumed conditions.

Another parameter of interest is the minimum detectable temperature difference, $\Delta T_{min}$, at some given target average temperature, $T_{avg}$. Since $\bar{N}_T(\text{eff})$ may be easily evaluated on a computer in 1°K increments, a list of $\bar{N}_T(\text{eff})$ values versus blackbody temperature may be tabulated over any temperature range of interest. This has been done from 100°K to 400°K. The change in effective radiance per degree of target temperature change is expressed as

$$\frac{\partial \bar{N}_T(\text{eff})}{\partial T} = \int_0^\infty RR_\lambda \, [N(\lambda, T+1) - N(\lambda, T)] d\lambda \quad . \tag{8}$$

Now, the ratio

$$\frac{\bar{N}_T'(\text{eff})}{\dfrac{\partial \bar{N}_T(\text{eff})}{\partial T}} = \Delta T_{min} \quad , \tag{9}$$

and when evaluated for T = 300°K, gives the minimum detectable temperature change, $\Delta T_{min}$, for targets around 300°K in temperature. Thus,

$$\Delta T_{\substack{min \\ \text{at } 300°K}} = \frac{\bar{N}'(\text{eff})}{\dfrac{\partial \bar{N}(\text{eff})}{T_{300}}} = \frac{2.63 \times 10^{-6} \text{ watt} \cdot \text{cm}^{-2} \cdot \text{sr}^{-1} \cdot °K}{2.50 \times 10^{-5} \text{ watts} \cdot \text{cm}^{-2} \cdot \text{sr}^{-1}} = 0.11°K \quad ,$$

$$\Delta T_{\substack{min \\ \text{at } 200°K}} = \frac{2.63 \times 10^{-6}}{6.5 \times 10^{-6}} = 0.40°K \quad ,$$

and

$$\Delta T_{\substack{\text{min} \\ \text{at } 400^\circ K}} = \frac{2.63 \times 10^{-6}}{4.22 \times 10^{-5}} = 0.06^\circ K \quad .$$

The variation in $\Delta T_{min}$ for different temperatures occurs because $\bar{N}_T(eff)$ is a function of target temperature and radiation wavelength as seen from equation (6b).

It should be noted that this analysis assumes the sky background temperature to be about 295°K because $NEP_\lambda$ was measured in a laboratory environment. A turbulent atmosphere would give rise to significantly higher background noise levels, which would increase the minimum detectable temperature as well as $\Delta T_{min}$. Conversely, a cold, quiescent atmosphere would be expected to give improved performance.

Examination of equation (6a) clearly shows the relationship of the output S/N to the various system parameters. It is seen that for a given target radiance, S/N is directly proportional to detector $D^*_\lambda$ and area and is inversely proportional to electrical bandwidth and system F-number. Improvements in $T_{min}$ and $\Delta T_{min}$ would require a detector having a better $D^*_\lambda$ or reduced electrical bandwidth. This latter change would, of course, reduce system response time and, therefore, data rate.

It should be mentioned that for a background noise limited detector, $D^*_\lambda$ is inversely proportional to the detector solid angular field of view and background temperature. If the detector field of view is cold-shielded to match the exit slope angle of the collecting optics, then $D^*_\lambda$ effectively becomes a function of system F-number. S/N would not actually vary as the square of the F-number in this case, since a decrease in $F_n$ requires an increase in the exit slope angle of the optical system. This in turn requires a corresponding increase in the detector cold-shielded field of view, which results in an increase in background noise. This fact would have to be considered in any estimate of S/N improvement to be gained by changing to a faster optical system. In many instances, instruments are designed with respect to an existing telescope that is available to the experimenter.

## Signal Processing

The ac signal from the detector is brought into a phase-lock amplifier and synchronously demodulated to give a 0- to ± 10-Vdc output. The output is recorded on a strip-chart recorder or magnetic tape. The amplifier has a variable post detection time constant, which may be increased for weak signals. An electronic zero offset is provided so that small signal differences riding on a large basic signal may be amplified and observed. A brief but clear explanation of synchronous detection may be found in Reference 2. Figure 5 shows a block diagram of the elements of a synchronous detection system.

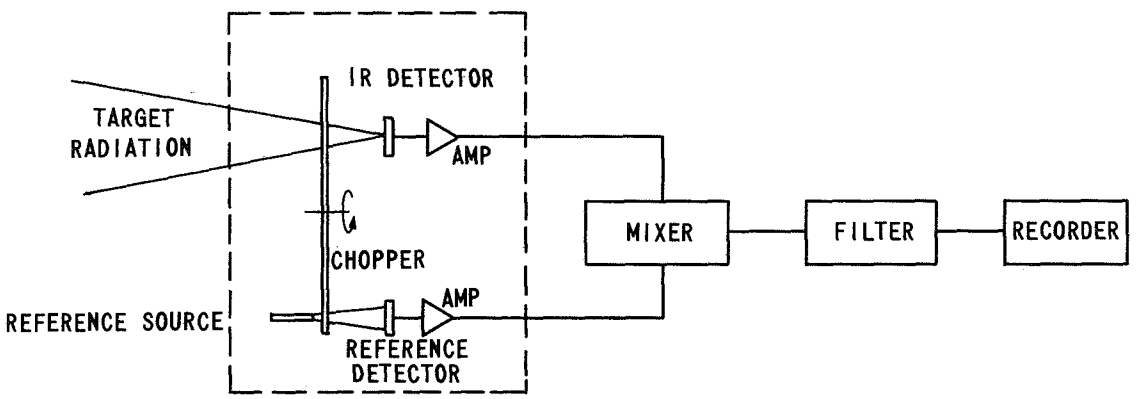


Figure 5. Elements of synchronous system.

## Mechanical Design

The following factors have been considered in the mechanical design of the radiometer:

1. It is rigid enough so that bending or flexing will not affect optical alignment.

2. It is sturdy enough to be transported from laboratory to observatory without affecting optical alignment.

3. It is lightweight enough to be mounted on a telescope by only two people.

4. Heat producing elements such as chopper motors are situated such that they do not enter the detector field of view.

5. Light producing elements such as mirror illuminators or reference sources are situated so that they do not enter the photomultiplier field of view.

6. The mounting of the dewar is such that the liquid coolant will not spill from the open top with the telescope in any position from vertical to near horizontal.

7. The radiometer should be rotatable about the telescope optical axis, and tolerances should be such that this rotation will cause negligible optical misalignment. This is very difficult to achieve, especially with instruments whose mass is not symmetrical about the optical axis. Future designs should provide an x-y adjustment of the entire radiometer while mounted to the telescope backplate. Under these conditions, any misalignment caused by instrument sagging or insignificant mechanical tolerance may be corrected by vernier screw adjustments.

8. All element mounts are accessible for adjustment.

# CALIBRATION AND DATA REDUCTION

## Calibration

The final form of a radiometric calibration technique is usually simple, after one has accurately measured the transmission and/or reflectance of all optical elements such as windows, mirrors, filters, beam splitters, etc.; has measured the relative response of the particular detector; has accurately determined the true field of view (as opposed to a calculated field); and has determined if changes in detector orientation or ambient pressure affect system response. Other effects, such as polarization and saturation effects, etc., should be measured if possible. If extreme caution and diligence for precision are practiced, one may expect a calibration error on the order of 1 or 2 percent.

For a radiometer such as this, it is preferable to make measurements simultaneously on an entire series of elements as they will be used in the system

rather than making individual measurements on separate elements. This is because interactions such as interference and multiple reflections can produce a significantly different throughput from that inferred by mathematically combining individually measured component characteristics.

The final step in radiometric calibration is a determination of the system responsivity, R, defined as the voltage (or current) output per unit radiant input. Of several methods available, the one described below was chosen for its simplicity and its relative ease of performance under the conditions imposed by observatory operation.

Two temperature-controllable blackbodies of identical design are mounted on a mechanical device (Fig. 6) which is placed on the radiometer when a calibration is desired. An accurately machined aperture, 1.52 cm in diameter, is located in the stationary base of the device and is positioned by guide pins directly above the entrance aperture of the radiometer coincident with the system optical axis. This aperture serves as the effective calibration blackbody aperture and is at an accurately measured distance from the detector. The two blackbodies can be moved quickly and accurately over the aperture using the slide arrangement shown in Figure 6. After the calibration temperatures of the two blackbodies have been set and allowed to stabilize for a minimum of 45 minutes, the detector voltage output is recorded for each blackbody in rapid succession. This completes the measurement portion of the calibration.

Two blackbodies are used at two preset temperatures, rather than setting a single one at several temperatures consecutively. This is because significant background radiation is received from the outer regions of the detector's field of view, and, as may be seen from equations (10) and (11), any change in this background radiation during calibration would introduce an indeterminable error into the output signal. The relatively long time required for a single blackbody to stabilize at different temperatures is an invitation to this type of error.

The dc voltage output of the phase lock amplifier is derived from the radiative contribution of several distinct sources. The peak-to-peak value of the square wave ac signal from the detector is proportional to the radiation received on alternate half cycles of the optical chopper. On the closed portion of the chop cycle, the detector "sees" radiation from the calibration blackbody as well as an unknown amount of radiation from the surrounding background (in some cases, this background contribution to the signal may even be greater than that from the calibration source). This may

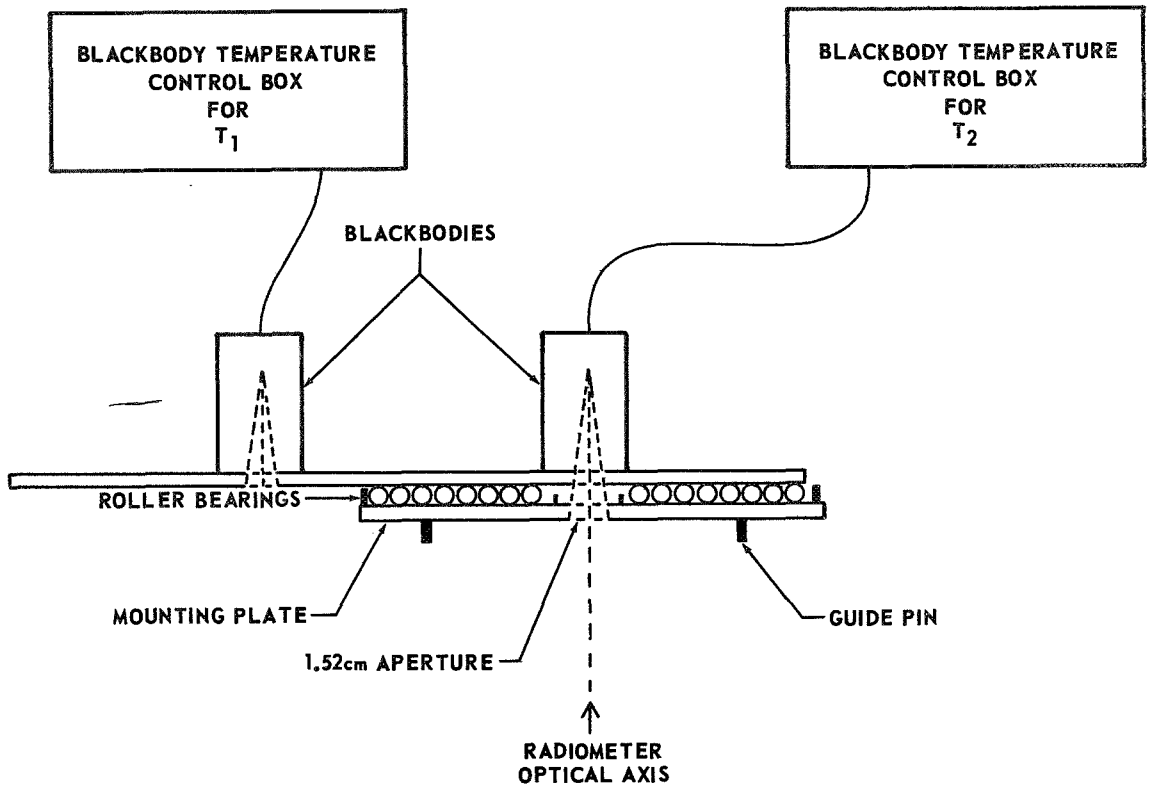


Figure 6. Calibration blackbody slide apparatus.

be symbolized as

$$V_{c_1} + V_{BG} = V_T \quad .$$

On the open half of the chop cycle, the detector sees the radiation from an internal reference source (or in some cases, simply the radiometer cavity radiation) which is symbolized by $V_I$. The magnitude and phase relation of the resulting ac signal is dependent on the difference $(V_T - V_I)$, which gives zero output when both are equal.

The rms output from the electronics when viewing calibration source (1) at temperature $T_1$ is then

$$V_1 = [(V_{c_1} + V_{BG}) - V_I]\alpha \quad ; \qquad (10)$$

and when viewing calibration source (2) at temperature $T_2$, the rms output is

$$V_2 = [V_{c_2} + V_{BG} - V_I]\alpha \quad , \tag{11}$$

where $\alpha$ is the Fourier coefficient of the chop waveform fundamental and is maximum for a square wave. Since the slide arrangement allows the two measurements to be made quickly, the assumption is made that the contributions to the signal from the background and internal reference remain constant during the measurements. Therefore, the voltage difference $(V_1 - V_2)$ is a result of the calibration sources temperature difference only.

Thus,

$$\Delta V_c = (V_1 - V_2) = [(V_{c_1} + V_{BG} - V_I) - (V_{c_2} + V_{BG} - V_I)] \cdot \alpha$$

$$\Delta V_c = (V_{c_1} - V_{c_2}) \cdot \alpha \quad , \tag{12}$$

where $\Delta V_c$ is termed the calibration signal. Referring to equation (4), the voltage difference between the two blackbodies may be expressed in terms of system parameters and radiometric quantities. This leads to

$$\Delta V_c = \Delta P_d(\text{eff}) \cdot R_{\lambda_p} = \frac{A_c \cdot A_d}{d^2} R_{\lambda_p} \int_0^\infty \frac{R_\lambda}{R_{\lambda_p}} \cdot \epsilon_c(\lambda) \cdot \tau_a(\lambda) \cdot \tau_f(\lambda)$$

$$\cdot \tau_w(\lambda) \cdot \rho_c(\lambda) \cdot [N_\lambda(\lambda, T_1) - N_\lambda(\lambda, T_2)]d\lambda \quad . \tag{13}$$

The functions $\tau_f(\lambda)$, $\tau_w(\lambda)$, and $\rho_c(\lambda)$ are all produced by permanent elements of the radiometer, and their absolute values are not required as long as absolute power measurements are not required. The relative spectral response of the system is required, however, to evaluate the integral. This function, normalized to its peak value, was obtained with the aid of a Perkin Elmer Model E-14 spectrometer and is shown in Figure 7.

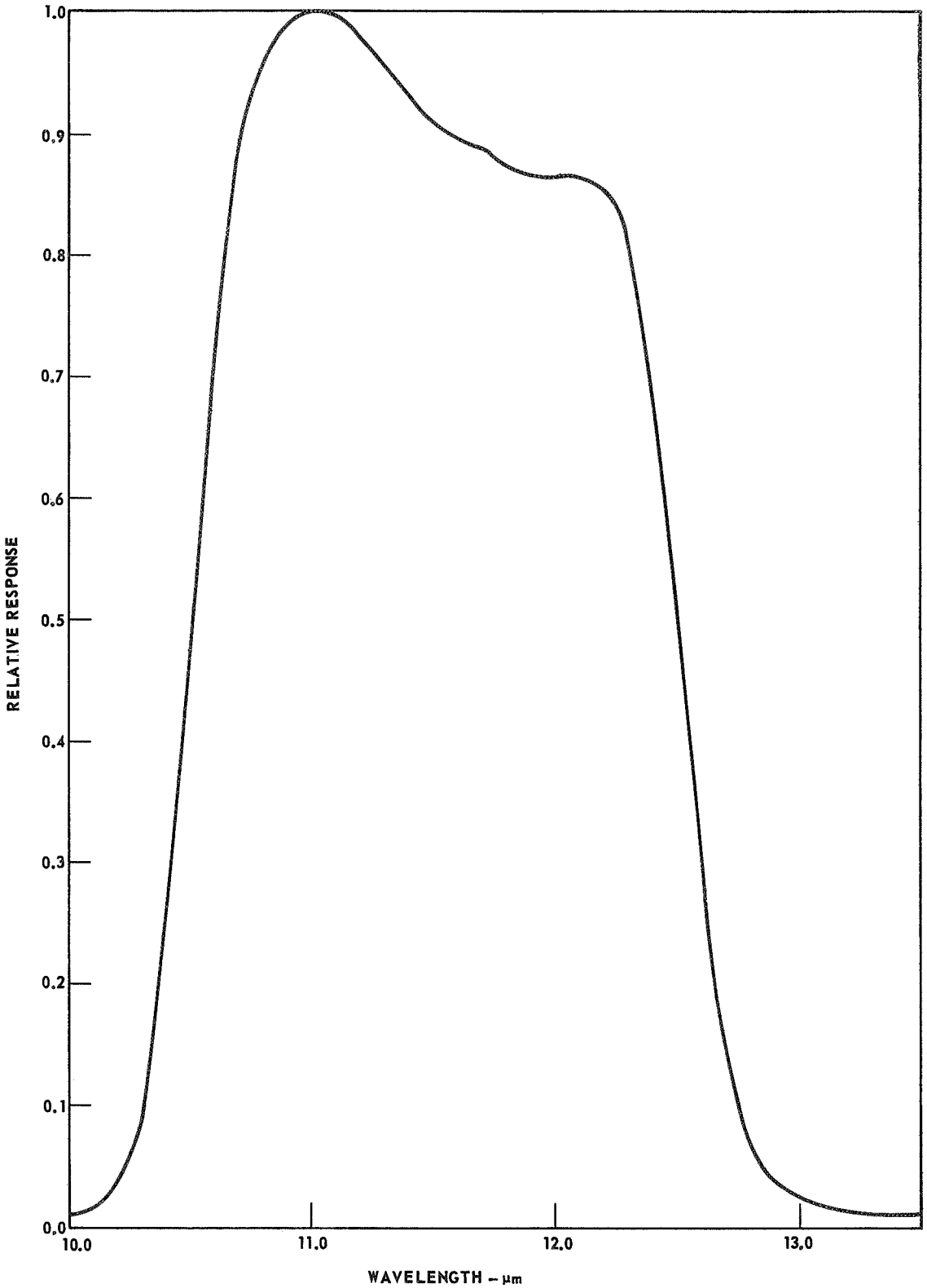


Figure 7. Relative response of system.

If $\tau_a(\lambda)$ is taken to be unity over the calibration distance d and $\epsilon_c(\lambda)$ is assumed to be constant over the spectral interval, these quantities may be brought outside the integral. It is convenient to define a quantity N(T), given by

$$N(T) = \int_0^\infty \frac{R_\lambda}{R_{\lambda_p}} \cdot N_\lambda(\lambda, T)\, d\lambda \quad , \tag{14}$$

where $\frac{R_\lambda}{R_{\lambda_p}}$ is the system response normalized to unity at the wavelength of peak response as shown in Figure 7. Equation (14) has been evaluated numerically and tabulated in 1°K increments from 50 to 500°K.

Rewriting equation (13) gives

$$\Delta V_c = \frac{A_c A_d}{d^2} \cdot \bar{\epsilon}_c R_{\lambda_p} [N(T_1) - N(T_2)] \quad , \tag{15}$$

which forms the basic calibration equation from which the system responsivity constant, $R_{\lambda_p}$, is evaluated. It would be possible to simulate telescope reflectance values during calibration by placing two mirrors, coated simultaneously with the telescope mirrors, in the calibration optical path, d. These mirrors would not be normal to the optical line of sight, however, and would require checks against possible polarization effects.

When viewing extended sources such as the moon, the factor $A_d$ occurs in both the calibration and data reduction equations so that equation (15) may be solved for the quantity $A_d R_{\lambda_p}$. If one lets $A_d R_{\lambda_p} = R_c$ and $\frac{A_c \bar{\epsilon}_c}{d^2} = c$, then the final form of the calibration equation is given by

$$R_c = \frac{\Delta V_c}{c \cdot [N(T_1) - N(T_2)]} \tag{16}$$

$R_c$ has units of volts · $cm^2$ · $watt^{-1}$ and is determined by the method described in this section for blackbody temperatures $T_1$ and $T_2$. A slightly different calibration technique would be to set the calibration blackbody to a number of different temperatures and plot the corresponding voltage outputs against $c \cdot N(T)$. The slope of the best fit straight line plot would then yield $R_c$. This method, however, is more time consuming and would be subject to the background change errors discussed previously.

The largest error associated with this method of calibration comes from inaccuracies in the measurement of the absolute temperatures of the calibration blackbodies.

## Data Reduction

Two separate measurements are required to extract the moon signal from the moon-plus-sky emission signal. As may be seen from Figure 8, the spectral radiance of a clear, cool night sky [2] at 11 $\mu$m is low, well below equivalent 0° C blackbody emission even at elevation angles as low as 10 deg. However, in regions of high humidity and warm temperatures, the sky radiance can exceed that of a 0° C blackbody at low elevation angles, as seen from the Cocoa Beach plot of Figure 8. The effect of increasing air mass on sky radiance and, hence, sky signal voltage may be seen from the curves for different elevation angles. Even the presence of unobservable (to the eye) clouds or haze can cause a significant variation in sky level readings from one part of the sky to another. Any change in general atmospheric conditions such as would result from the invasion of a cold or warm front or the influx of a humid air mass will show itself as a change in shape on plots of sky radiance versus elevation angle as a function of time. If the change is rapid, an obvious change in radiometric output could be observed at a given elevation angle. These effects can cause quite a problem in the determination of nightly extinction, where data have been taken over long observation periods (4 to 8 hours).

The contribution to the total signal from sky emission may be eliminated simply by observing the sky at a given zenith angle in the moon's path and recording the system voltage output. As the moon drifts into the field of view, its contribution to the signal is added to that of the sky; thus, the difference between the two voltage levels is because of the moon alone. As long as this process does not take too long (on the order of 2 or 3 minutes), variations in sky emission may be considered negligible, except as a

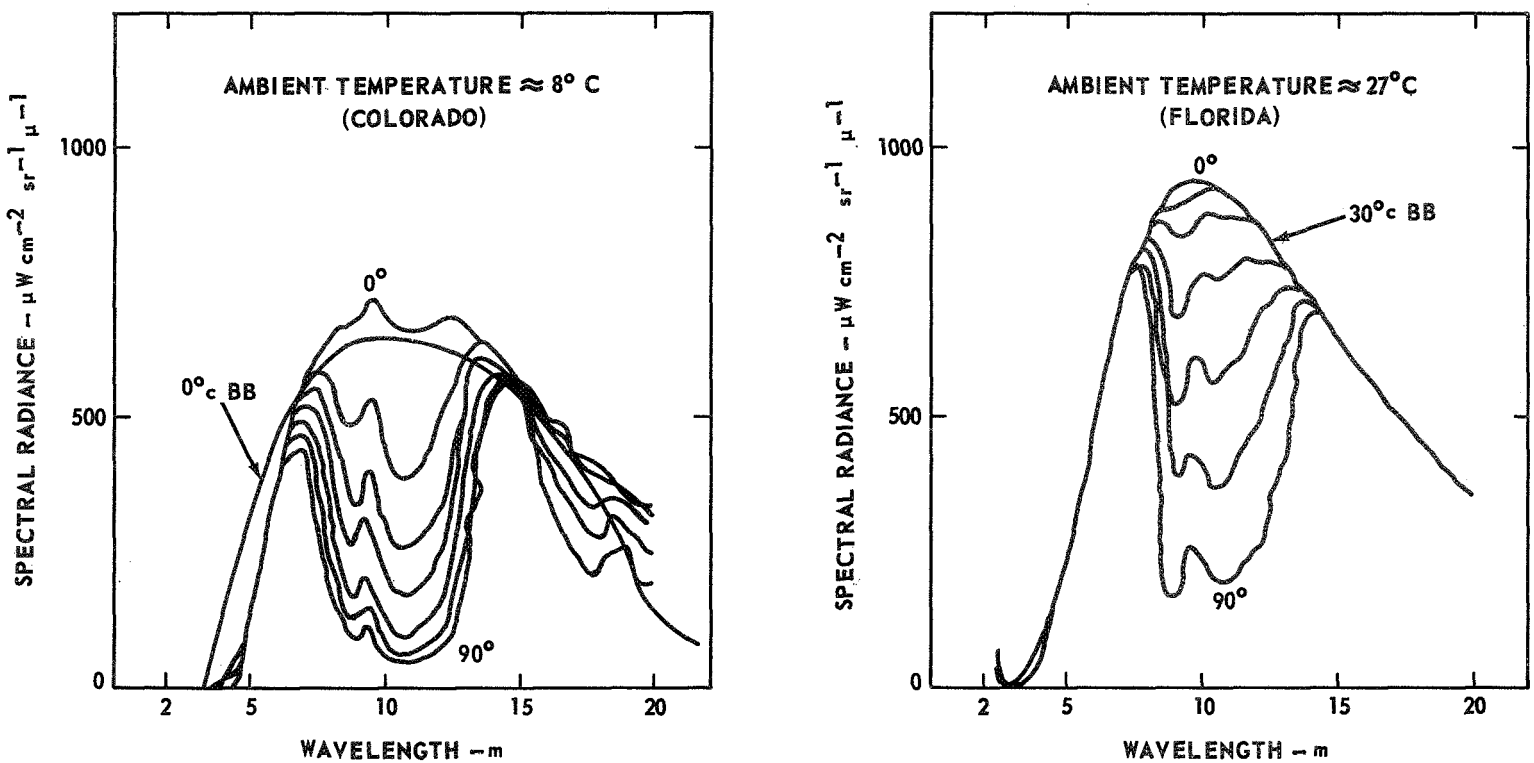


Figure 8. Spectral radiance of clear night sky.

contribution to system noise. Another effect that may be significant during a drift scan is the contribution to the signal from radiation scattered into the detector as the bright limb drifts near the radiometer field of view. The effect of this scattered radiation would be to increase the sky level reading to a level slightly higher than the true sky level. This scattering effect is greater at large zenith angles, since the density of scattering particles along the slant path is greatest. The magnitude of this effect can be measured by pointing the radiometer field of view sufficiently ahead of the travel path of the moon to assure that scattering effects are not present and monitoring an expanded scale output of sky level voltage as the moon approaches. When the surface of the moon is fully in the field of view, errors because of scattering effects would be minimal, since, statistically, radiation scattered in and out of the field would be about equal for an extended source.

Data reduction consists of determining a blackbody radiance value $N(T_m)$ for the moon and comparing this value with the tabulated list of $N(T)$ values as determined from equation (14). A list of system $N(T)$ values with their corresponding temperatures is shown in Table 2 for temperatures near 400°K.

TABLE 2. SYSTEM N(T) VALUES

| N(T) Watts · cm$^{-2}$ · sr$^{-1}$ | T °K |
|---|---|
| $4.658 \times 10^{-3}$ | 390 |
| $4.699 \times 10^{-3}$ | 391 |
| $4.740 \times 10^{-3}$ | 392 |
| $4.781 \times 10^{-3}$ | 393 |
| $4.822 \times 10^{-3}$ | 394 |
| $4.864 \times 10^{-3}$ | 395 |
| $5.073 \times 10^{-3}$ | 400 |

The voltage output of the system for the moon is given by the expression,

$$V_{(m)} = \frac{A_t \cdot \overline{\rho}_t^{\,2} \cdot \overline{\tau}(a)}{f_t^{\,2}} \cdot \overline{\epsilon}_m \, N(T_m) \cdot R_c \quad ,$$

where $V_{(m)} = V_{s+m} - V_s$ .

Solving this equation for $N(T_m)$ and substituting from equation (16) for $R_c$ gives the desired data reduction equation ,

$$N(T_m) = \frac{f_t^{\,2} (V_{m+s} - V_s) \cdot c \cdot [N(T_1) - N(T_2)]}{A_t \, \overline{\rho}_t^{\,2} \cdot \overline{\tau}(a) \cdot \Delta V_c \cdot \overline{\epsilon}_m} \qquad (18)$$

$\Delta V_c$ is measured directly for calibration blackbody temperatures $T_1$ and $T_2$, and the corresponding values for $N(T_1)$ and $N(T_2)$ are taken from the listing of $N(T)$ values. $V_{m+s}$ and $V_s$ are the system output voltages developed when viewing the moon and sky respectively through a telescope of effective collecting area $A_t$, focal length f, and mirror reflectance $\rho_t$. The atmospheric transmission is determined separately, as a function of air mass, by using the "weak-line approximation" [3] model, and a reference point on the moon as the extinction source. $N(T_m)$ is the calculated effective radiance value of that area of the moon filling the system field of view and is convertible to a radiometric temperature, given a value for $\overline{\epsilon}_m$. If $\overline{\epsilon}_m$ is taken to be 1, the temperature is then termed brightness temperature. If the goniometric emission characteristics of the area observed is Lambertian, then the true temperature would be greater by a factor of $1/\overline{\epsilon}_t$, where $\overline{\epsilon}_t$ is the true hemispherical emissivity of the surface averaged over the spectral bandpass of the system.

Two methods of data reduction will be illustrated using the data reproduced in Figures 9 and 10. Figure 9 represents an analog voltage plot of radiation measured from a selected site on the lunar surface, in this case the crater Bruce near the disc center. The radiometer/telescope was visually

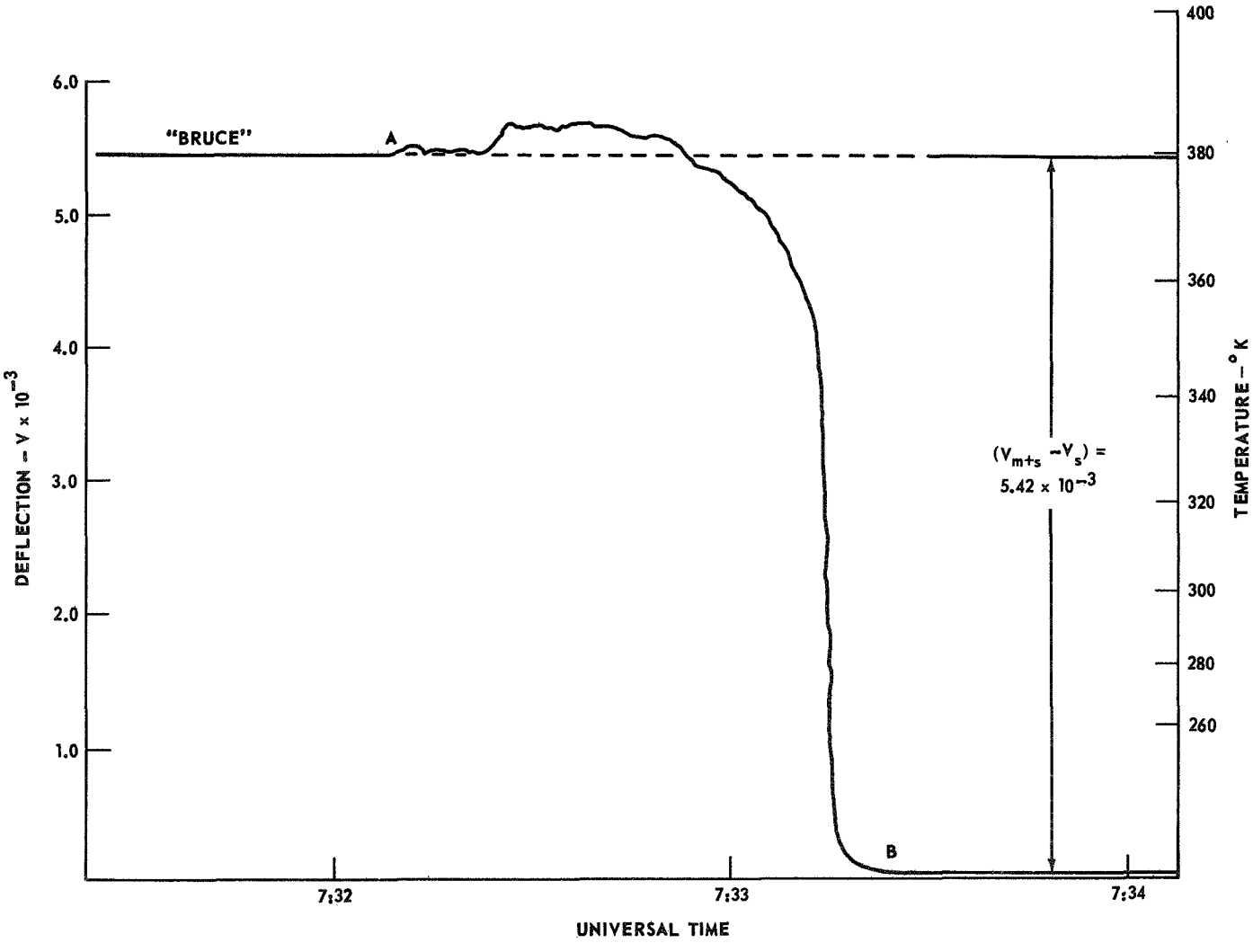


Figure 9. Analog plot of radiometric signal from the crater Bruce.

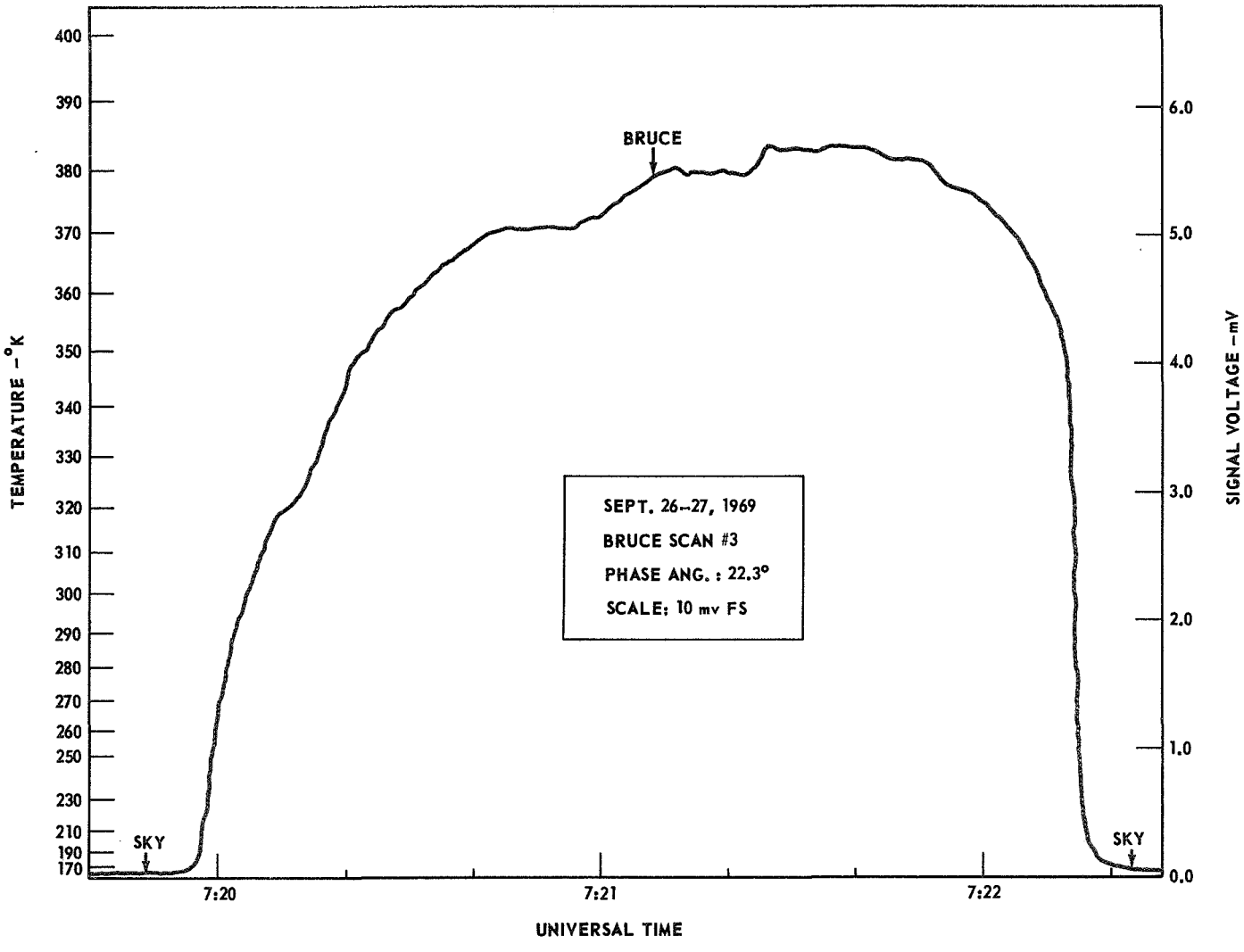


Figure 10. Analog plot of lunar drift scan.

pointed at the site by means of the reflex optics and allowed to track the point for approximately 5 seconds. The RA drive is disengaged at point A, and the moon drifts out of the field of view. This takes about 1 minute, during which time it is assumed that atmospheric emission and transmission remain relatively constant. As the moon's limb leaves the field of view, the signal drops rapidly to sky level B, which is recorded for an additional 30 seconds. The signal from the moon $(V_{m+s} - V_s)$ is determined by direct measurement from the strip chart. Time is recorded so that the zenith angle for the site Bruce may be determined from the lunar ephemeris and applied to the calculation of air mass for which $\overline{\tau}_a$ is determined.

$(V_{m+s} - V_s)$ and $\overline{\tau}_a$ are entered into equation (18) along with the system constants and calibration data, and $N(T_m)$ is calculated for a 40 km diameter area around the crater Bruce. A computer program has been written for the Univac 1108 which will print out the temperature corresponding to the nearest $N(T_m)$ value that it has in core storage. This is a brightness temperature that can be corrected for $\overline{\epsilon}_t$ should such value ever become available for the area under measurement. The system propagation of error analysis in the next section shows that with the present system, the probable error in a single brightness temperature measurement of this type is approximately $\pm 8°K$.

Figure 10 represents the analog output of the system for a drift scan of the disc. The same procedure of scanning is used except the telescope is driven to some point in the sky ahead of the moon. The right ascension drive is disengaged allowing the moon to drift across the stationary field of view. A full disc scan requires about 2 minutes plus an additional 30 seconds of sky on each end of the scan. One advantage to this method of scanning is that air mass remains constant, simplifying $\overline{\tau}_a$ calculations. During the course of the scan, photographs are taken through the radiometer optical system to pinpoint the scan on a separate full phase photograph. Assuming a 21 arc sec field of view, about 100 contiguous scans would be required to completely scan the moon using this procedure. If an average of 3 minutes is allowed per scan, then a complete scan program of the full disc would require 5 hours.

A temperature scale may be derived for this type of data in the following manner. The data reduction equation is solved by inputting a range of values for $N(T_m)$ and calculating a corresponding list of

$(V_{m+s} - V_s)$ values. These values are printed out in either 1° or 10° increments of temperature versus voltage for each scan. The temperature scale may then be applied directly to the strip chart voltage trace as shown in Figure 10. Figure 11 shows an expanded scale scan of the central portion of the disc using the electronic offset feature of the synchronous detection system.

# ERROR ANALYSIS

## Propagation of Error Equation

A radiometric measurement of temperature actually requires the individual measurement of a number of other quantities from which the temperature value is calculated. To determine the probable error associated with this temperature value, one must know how the inaccuracies associated with the determinations of these other quantities contribute to the inaccuracy of the result.

The system propagation of error equation derived below shows the contribution of the individual component errors to the overall temperature error. Where possible, the probable errors associated with the individual components were derived by standard statistical means. On items where measurements were not feasible, best estimates of error are used.

Following the method used by Ingrao [4], the data reduction equation, which is an expression for the radiance of the moon as measured by the system, is expressed in general form similar to the Stefan-Boltzmann law as

$$N(T_m) = A\,T_m^{B} \quad , \tag{19}$$

where A and B may be assumed constants over the range of temperatures expected on the sunlit portion of the lunar disc. Differentiation of this equation with respect to $T_m$ gives

$$dN(T_m) = ABT_{(m)}^{B-1}\,dT_m \tag{20}$$

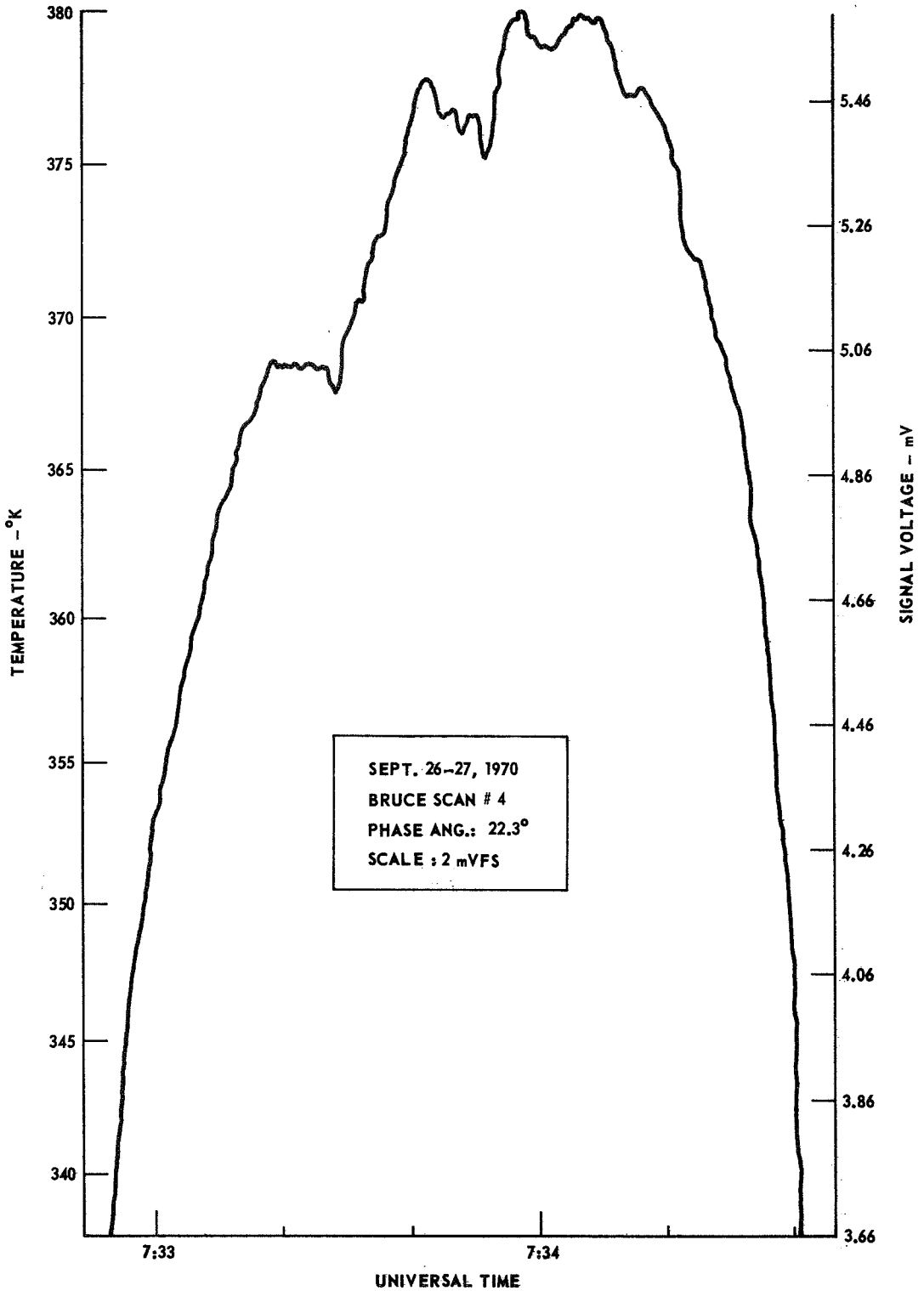


Figure 11. Expanded scale scan of a portion of lunar disc.

Replacing A with $\frac{N(T_m)}{T_m^B}$ leads to

$$\frac{dT_m}{T_m} = \frac{1}{B} \cdot \frac{dN(T_m)}{N(T_m)} \tag{21}$$

or

$$\frac{dT_m}{T_m} = \left[ \frac{N(T_m)}{T_m} \cdot \frac{dT_m}{dN(T_m)} \right] \frac{dN(T_m)}{N(T_m)}$$

If the errors in $N(T_m)$ and $T_m$ are small, the following approximation is valid [5]:

$$\frac{\Delta T_m}{T_m} = \left[ \frac{N(T_m)}{T_m} \cdot \frac{dT_m}{dN(T_m)} \right] \frac{\Delta N(T_m)}{N(T_m)} \tag{22}$$

The weighting factor $\left[ \frac{N(T_m)}{T_m} \cdot \frac{dT_m}{dN(T_m)} \right]$ may be evaluated using the pretabulated tables of T versus N(T), and the expression for $\frac{\Delta N(T_m)}{N(T_m)}$ may be determined by differentiating equation (18). This leads to the expression,

$$\begin{aligned}\frac{\Delta T_m}{T_m} = &\left[ \frac{N(T_m)}{T_m} \cdot \frac{dT_m}{dN(T_m)} \right] \\ &\cdot \left\{ \left| \frac{\Delta(V_{m+s}-V_s)}{V_{m+s}-V_s} \right| + \left| \frac{\Delta A_c}{A_c} \right| + \left| \frac{\Delta \epsilon_c}{\epsilon_c} \right| + 2 \left| \frac{\Delta f_t}{f_t} \right| + \left| \frac{\Delta A_t}{A_t} \right| + \left| \frac{\Delta \epsilon_m}{\epsilon_m} \right| \right. \\ &+ \left| \frac{\Delta \tau_a}{\tau_a} \right| + 2 \left| \frac{\Delta \rho_t}{\rho_t} \right| + 2 \left| \frac{\Delta d}{d} \right| + \left| \frac{\Delta(V_1-V_2)}{V_1-V_2} \right| + \left| \left( \frac{dN}{dT} \right)_{T_1} \frac{\Delta T_1}{N(T_1)-N(T_2)} \right| \\ &\left. + \left| \frac{dN}{dT}_{T_2} \frac{\Delta T_2}{N(T_1)-N(T_2)} \right| \right\} .\end{aligned} \tag{23}$$

Evaluation of this expression with maximum expected fractional error values entered for the components of the second bracket would yield the maximum fractional error expected for a single temperature measurement.

By defining the probable error of a single temperature measurement of the moon in a manner analogous to the standard deviation (i.e., the square root of the sum of the squares of the individual probable errors) equation (23) may be expressed as

$$\left(\frac{\Delta T_m}{T_m}\right)_{prob} = \left[\frac{N(T_m)}{T_m} \cdot \frac{dT_m}{dN(T_m)}\right] \cdot \left\{\left(\frac{\Delta(V_{m+s}-V_s)}{V_{m+s}-V_s}\right)^2 + \left(\frac{\Delta A_c}{A_c}\right)^2 + \left(\frac{\Delta \epsilon_c}{\epsilon_c}\right)^2 + 4\left(\frac{\Delta f_t}{f_t}\right)^2 + \left(\frac{\Delta A_t}{A_t}\right)^2 + \left(\frac{\Delta \epsilon_m}{\epsilon_m}\right)^2 + \left(\frac{\Delta \tau_a}{\tau_a}\right)^2 + 4\left(\frac{\Delta \rho_t}{\rho_t}\right)^2 + 4\left(\frac{\Delta d}{d}\right)^2 + \left(\frac{\Delta(V_1-V_2)}{V_1-V_2}\right)^2 + \left[\left(\frac{dN}{dT}\right)_{T_1} \frac{\Delta T_1}{N(T_1)-N(T_2)}\right]^2 + \left[\left(\frac{dN}{dT}\right)_{T_2} \frac{\Delta T_2}{N(T_1)-N(T_2)}\right]^2\right\}^{1/2} \quad (24)$$

In this case, the values entered into the second bracket would be the fractional probable errors derived for the individual components.

## Error Derivation

The probable error has been evaluated based on Table 3. The probable error is evaluated at two lunar temperatures, $T_m$ = 400°K and 200°K. Blackbody calibration temperatures are taken to be $T_1$ = 400°K and $T_2$ = 300°K.

TABLE 3. FRACTIONAL ERROR VALUES

| Component | | Fractional Error |
|---|---|---|
| (1) | $\frac{\Delta(V_{m+s}-V_s)}{V_{m+s}-V_s}$ | ± 0.01 |
| (2) | $\frac{\Delta A_c}{A_c}$ | ± 0.001 |
| (3) | $\frac{\Delta \epsilon_c}{\epsilon_c}$ | ± 0.01 |
| (4) | $\frac{\Delta f_t}{f_t}$ | ± 0.01 |
| (5) | $\frac{\Delta A_t}{A_t}$ | ± 0.01 |
| (6) | $\frac{\Delta \epsilon_m}{\epsilon_m}$ | ± 0.03 |
| (7) | $\frac{\Delta \tau_a}{\tau_a}$ | ± 0.03 |
| (8) | $\frac{\Delta \rho_t}{\rho_t}$ | ± 0.02 |
| (9) | $\frac{\Delta d}{d}$ | ± 0.0025 |
| (10) | $\frac{\Delta(V_1-V_2)}{V_1-V_2}$ | ± 0.01 |
| (11) | $\Delta T_1$ | ± 0.25°K |
| (12) | $\Delta T_2$ | ± 0.25°K |

For $T_m = 400°K$,

$$\frac{N_{T_{(400)}}}{T_{(400)}} = \frac{5.073 \times 10^{-3}}{4 \times 10^{2}} = 1.268 \times 10^{-5}$$

$$\frac{dT_{(400)}}{dN} = 2.37 \times 10^{4}$$

$$\frac{dN_{T_{(400)}}}{dT_{(400)}} = 4.219 \times 10^{-5}$$

$$\frac{dN_{T_{(300)}}}{dT_{(300)}} = 2.447 \times 10^{-5}$$

$$\left( \frac{N_{T_{(400)}}}{T} \cdot \frac{dT_{(400)}}{dN} \right) = 0.3048$$

$$N_{T_{(400)}} = 5.073 \times 10^{-3}$$

$$N_{T_{(300)}} = 1.706 \times 10^{-3}$$

$$\frac{dN}{dT_{(400)}} \cdot \frac{1}{[N(400) - N(300)]} = \frac{4.219 \times 10^{-5}}{3.367 \times 10^{-3}} = 1.258 \times 10^{-2}$$

$$\frac{dN}{dT_{(300)}} \cdot \frac{1}{[N(400) - N(300)]} = \frac{2.447 \times 10^{-5}}{3.367 \times 10^{-3}} = 7.98 \times 10^{-3}$$

$$\left( \frac{\Delta T}{T_{(400)}} \right)_{prob} = (0.305)[(0.01)^2 + (0.001)^2 + (0.01)^2 + 4(0.01)^2 + (0.01)^2 + (0.03)^2 + (0.03)^2 + 4(0.02)^2 + 4(0.0025)^2 + (0.01)^2 + (1.258 \times 10^{-2} \times 0.25)^2 + (7.98 \times 10^{-3} \times 0.25)^2]^{1/2}$$

$$\left(\frac{\Delta T}{T_{(400)}}\right)_{prob} = (0.305)\ (0.0648) = 0.0197 = \pm\ 1.97\%$$

$$\text{or} \quad \pm 7.9°K \quad .$$

The same analysis assuming $T_m = 200°K$ results in a probable error of $\pm 1.01$ percent or $\pm 2°K$. This is because of the fact that for the colder temperature, the factor $\frac{N(T_m)}{T_m} \cdot \frac{dT_m}{dN(T_m)}$ is reduced from 0.305 to 0.156. This estimate is probably somewhat optimistic, however, since for the low temperature radiation, greater uncertainties in the measurement of atmospheric transmittance and decreased signal-to-noise ratio of the moon signal would cause the probable errors of these components to be increased. In both cases, the analysis assumes good observing conditions.

From the error analysis, it is evident that a major source of error could be eliminated by calibrating the system through the telescope optics. This would eliminate the factors $4\left(\frac{\Delta f_t}{f_t}\right)$, $\frac{\Delta A_t}{A_t}$, and $4\left(\frac{\Delta \rho_t}{\rho_t}\right)$ from equation (6). However, with the present Cassegranian systems, a special calibration technique such as the Jones [6] method must be employed. This method is difficult and time consuming to set up and perform, and is not conducive to observatory conditions where night-to-night variations in system responsivity require frequent calibrations. For these reasons such an approach has not been adopted.

# REFERENCES


1. Bucher, G. C. and Stern, H. E., eds.: Physics of the Moon-Selected Topics Concerning Lunar Exploration. NASA TN D-2944, 1965.

2. Plass, G. N. and Yates, H.; Wolf, W. L., ed.: Handbook of Military Infrared Technology. Department of the Navy, Office of Naval Research, Washington, D. C., 1965.

3. Raine, W. L. and Landrum, S. M., Jr.: Use of a Direct-Imaging Filtered Radiometer for the Measurement of Lunar Brightness Temperatures. Summary Report No. RL-SSL-437, Contract No. NAS8-20166.

4. Ingrao, H. C.; Young, A. T.; and Lansky, J. L.: A Critical Analysis of Lunar Temperature Measurements in the Infrared. Harvard Coll. Obs. Scientific Rept. No. 6, NASA Research Grant No. NsG 64-60, 1965.

5. Young, H. D.: Statistical Treatment of Experimental Data. McGraw-Hill, New York, 1962.

6. Holter, M. R.; Nudelman, S.; Suits, G. H.; Wolfe, W. L.; and Zissis, G. J.: Fundamentals of Infrared Technology. The MacMillan Co., New York, 1962.

# APPROVAL

TM X-64539

# DESIGN AND DEVELOPMENT OF A LUNAR RADIOMETER

By Walter Fountain

The information in this report has been reviewed for security classification. Review of any information concerning Department of Defense or Atomic Energy Commission programs has been made by the MSFC Security Classification Officer. This report, in its entirety, has been determined to be unclassified.

This document has also been reviewed and approved for technical accuracy.

William C. Snoddy

WILLIAM C. SNODDY
Chief, Space Thermophysics Division

Gerhard B. Heller

GERHARD B. HELLER
Director, Space Sciences Laboratory

# DISTRIBUTION



INTERNAL

DIR
Dr. Rees

DEP-T
Mr. Neubert

AD-S
Dr. Stuhlinger

S&E-SSL-DIR
Mr. Heller
Mr. Hembree

S&E-SSL-C
Reserve (15)

S&E-SSL-N
Dr. Decher

S&E-SSL-P
Dr. Naumann

S&E-SSL-S
Dr. Seiber

S&E-SSL-T
Mr. Snoddy
Dr. Schocken

S&E-SSL-TE
Mr. Miller
Mr. Atkins
Mr. Fields
Mr. Reynolds
Mr. J. Fountain
Mr. Walter Fountain (15)
Mr. Duncan
Mr. Baugher
Mr. Reichmann
Mr. Wilson

S&E-SSL-TR
Mr. Arnett
Mr. Bannister
Mr. Zwiener
Dr. Kroes
Mr. Linton
Mr. Wilkes
Miss Richard
Dr. Kulshreshtha

S&E-SSL-TT
Mr. Jones
Mr. Gates
Mr. Craven
Dr. Gary
Dr. Hagyard
Mr. Watkins
Mr. Calvert

A&TS-MS-H
A&TS-MS-IL (8)
A&TS-MS-IP (2)

A&TS-PAT
Mr. L. D. Wofford, Jr.

A&TS-TU (6)
PM-PR-M

EXTERNAL

Scientific and Technical Information
Facility (25)
P. O. Box 33
College Park, Maryland 20740
Attn: NASA Representative (S-AK/RKT)



MSFC—RSA, Ala